Acta Crystallographica Section F
Structural Biology and Crystallization Communications
ISSN 1744-3091

Purification, crystallization and preliminary X-ray crystallographic analysis of mammalian MSS4–Rab8 GTPase protein complex

Aymelt Itzen, Nathalie Bleimling, Alexander Ignatev, Olena Pylypenko and Alexey Rak*

Max-Planck-Institute for Molecular Physiology, Otto-Hahn-Strasse 11, 44227 Dortmund, Germany

Correspondence e-mail: rak@mpi-dortmund.mpg.de

Received 15 November 2005
Accepted 22 December 2005

Rab GTPases function as ubiquitous key regulators of membrane-vesicle transport in eukaryotic cells. MSS4 is an evolutionarily conserved protein that binds to exocytotic Rabs and facilitates nucleotide release. The MSS4 protein in complex with nucleotide-free Rab8 GTPase has been purified and crystallized in a form suitable for structure analysis. The crystals belonged to space group $P1$, with unit-cell parameters $a = 40.92$, $b = 49.85$, $c = 83.48$ Å, $\alpha = 102.88$, $\beta = 97.46$, $\gamma = 90.12^\circ$. A complete data set has been collected to 2 Å resolution.

1. Introduction

Rabs form the largest protein group of the Ras superfamily of small GTP-binding proteins (Colicelli, 2004). The small GTPases of the Rab family control directional vesicle-mediated exchange of substances between different compartments in eukaryotic cells (Lazar *et al.*, 1997; Novick & Zerial, 1997; Waters & Pfeffer, 1999). Rab proteins are themselves tightly regulated at multiple levels, including expression, localization and activation, by switching between two functionally distinct conformations controlled by the state of the bound nucleotide. In the active GTP-bound state, they interact in a specific manner with downstream effector proteins, whereas in the GDP-bound state these interactions do not occur as a result of a conformational rearrangement that takes place upon GTP hydrolysis. This functional cycle is tightly controlled *via* the interaction with guanosine nucleotide-exchange factors (GEFs), which stimulate the exchange of GDP for GTP, and GTPase-activating proteins (GAPs), which specifically turn off the active state of the Rab protein by accelerating the slow intrinsic GTPase activity.

Mutations in the Rab GTPases or interacting proteins have been implicated in a number of human diseases including immunological and pigmentation disorders (Griscelli syndrome), mental retardation, neuropathy (Charcot–Marie–Tooth), kidney disease (tuberous sclerosis) and blindness (choroideremia) (Stein *et al.*, 2003). Moreover, in a number of vascular, lung and thyroid diseases as well as in some cancer forms the overexpression of several Rab GTPases is observed and correlates with disease progression (Stein *et al.*, 2003). Thus, investigation of the Rab-regulation machinery is a subject of a great interest. A number of Rab protein structures have been solved as well as Rab–effector complexes (reviewed in Eathiraj *et al.*, 2005). Recently, structures of Rab proteins in complexes with their generic regulators Rab-escort protein and Rab GDP dissociation inhibitors have been published (Rak *et al.*, 2003, 2004). Whereas GAPs and GEFs for Ras-family members have been studied in great detail (for a review, see Colicelli, 2004), there is only a limited amount of information on the corresponding GTPase-cycle regulators of Rab proteins (Rak *et al.*, 2000; Yu & Schreiber, 1995*a*; Zhu, Dumas *et al.*, 2001). MSS4 is a zinc-binding protein (Collins *et al.*, 1997) with GEF activity towards exocytotic Rab GTPases (Burton *et al.*, 1993; Burton & De Camilli, 1994). Homologues of MSS4 are present in evolutionarily diverse species including both fission and budding yeast (where it is called DSS4, dominant suppressor of Sec4), worms, flies, zebra fish and mammals (Zhu, Dumas *et al.*, 2001). Similar to known GEFs, they bind tightly to the nucleotide-free forms of exocytotic Rab GTPases (Burton *et al.*, 1993, 1994). However, in contrast to the

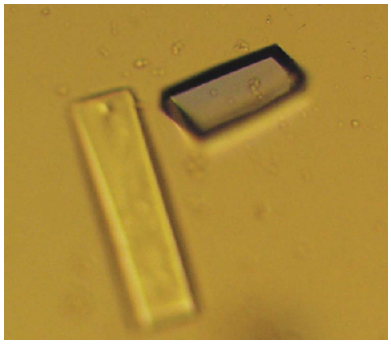

known GEF–GTPase complexes, which dissociate in the presence of GDP or GTP, MSS4 forms a long-lived complex with its cognate Rabs which is still relatively stable in the presence of high guanine-nucleotide concentration.

The structure of MSS4 has been solved by both X-ray (Zhu, Dumas *et al.*, 2001) and NMR (Yu & Schreiber, 1995*a*) methods and extensive mutagenesis analysis has been performed to identify the regions of Rab proteins and MSS4 proteins that take part in the interaction (Zhu, Delprato *et al.*, 2001). The availability of an MSS4–Rab complex structure will allow us to understand the unique biochemical properties of the MSS4/DSS4 protein family and to clarify their mechanism of action.

2. Experimental procedures

2.1. Cloning

To increase the likelihood of protein complex crystallization, the flexible regions of MSS4 and Rab8 were removed during cloning. A construct of human MSS4 (corresponding to residues 9–123) was amplified by PCR, digested with *Nde*I and *Xho*I and subcloned into a modified pET19 vector containing an N-terminal His_6 tag followed by a tobacco etch virus protease cleavage site. A construct of mouse Rab8 (the sequence identity between human and mouse Rab8 is 97%) corresponding to residues 1–183 was amplified by PCR, digested with *Nde*I and *Xho*I and subcloned into pET30a vector, which leads to an untagged protein. The MSS4 construct eliminates an N-terminal hypervariable extension that is poorly ordered in the NMR structure (Yu & Schreiber, 1995*b*). The Rab8 construct corresponds to the GTPase domain and lacks the C-terminal hypervariable region. Hereafter, these constructs will be termed MSS4 and Rab8, respectively.

2.2. Protein expression and purification

The MSS4 and Rab8 constructs were coexpressed in *Escherichia coli* BL21(DE3)RIL. Cells were grown in LB medium containing 34 µg ml^{-1} chloramphenicol, 125 µg ml^{-1} ampicillin and 50 µg ml^{-1} kanamycin at 310 K and were induced with 1 m*M* IPTG on reaching an $OD_{600\,nm}$ of 0.6. Cells were then grown for 17 h at 296 K. Cells were harvested, washed with PBS, resuspended in lysis buffer [25 m*M* sodium phosphate buffer (NaP_i) pH 7.5, 300 m*M* NaCl, 1 m*M* protease inhibitor PMSF, 10%(*v*/*v*) glycerol] and disrupted using a microfluidizer and 1%(*v*/*v*) Triton X-100 was added. After centrifugation (100 000*g*), the filtered supernatant was loaded onto a HiTrap Chelating HP column (GE) equilibrated with buffer *A* [25 m*M* NaP_i pH 7.5, 300 m*M* NaCl, 1 m*M* $MgCl_2$, 10 µ*M* GDP, 10%(*v*/*v*) glycerol]. After elution with a linear imidazole gradient (0–500 m*M* imidazole), the complex-containing fractions were pooled. The His_6 tag was removed with His_6-tagged TEV protease (1:20 protein:protease molar ratio) during overnight dialysis against 25 m*M* NaP_i pH 7.5, 300 m*M* NaCl, 1 m*M* $MgCl_2$, 10 µ*M* GDP, 10%(*v*/*v*) glycerol, 2 m*M* β-mercaptoethanol at 277 K. TEV protease and uncleaved protein were removed by passing the solution over a nickel–NTA column and the concentrated sample was subjected to size-exclusion chromatography on Superdex75 media [buffer: 10 m*M* HEPES pH 7.5, 100 m*M* NaCl, 1 m*M* $MgCl_2$, 5 µ*M* GDP, 2 m*M* β-mercaptoethanol, 5%(*v*/*v*) glycerol] (Fig. 1). Samples containing the protein complex were pooled, concentrated to 5.5 mg ml^{-1}, flash-frozen in liquid nitrogen and stored at 193 K.

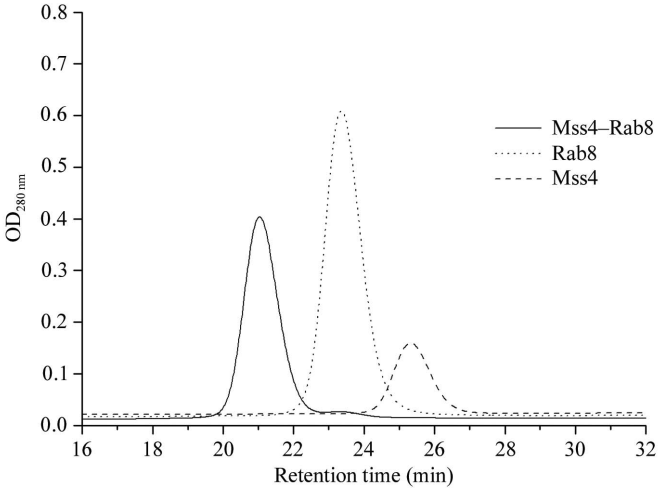

Figure 1
Analysis of MSS4–Rab8 complex formation by size-exclusion chromatography on a Superdex75 10/30 column. The figure demonstrates the increase in molecular size of MSS4 and Rab8 when forming the MSS4–Rab8 complex.

2.3. Crystallization

For crystallization screening, 96-well Greiner crystallization plates were used. Typically, 1 µl of 5.5 mg ml^{-1} protein solution was mixed with 1 µl reservoir solution and used as a sitting drop against 75 µl reservoir solution. Initial bundles of microcrystals were obtained in 2 days at 293 K in condition No. 36 of PEG/Ion Screen (Hampton Research) containing 0.2 *M* disodium tartrate and 20%(*w*/*v*) PEG 3350 (Fig. 2*a*). The crystal quality was improved by optimization of the crystallization conditions and by using 1,2,3-heptanetriole

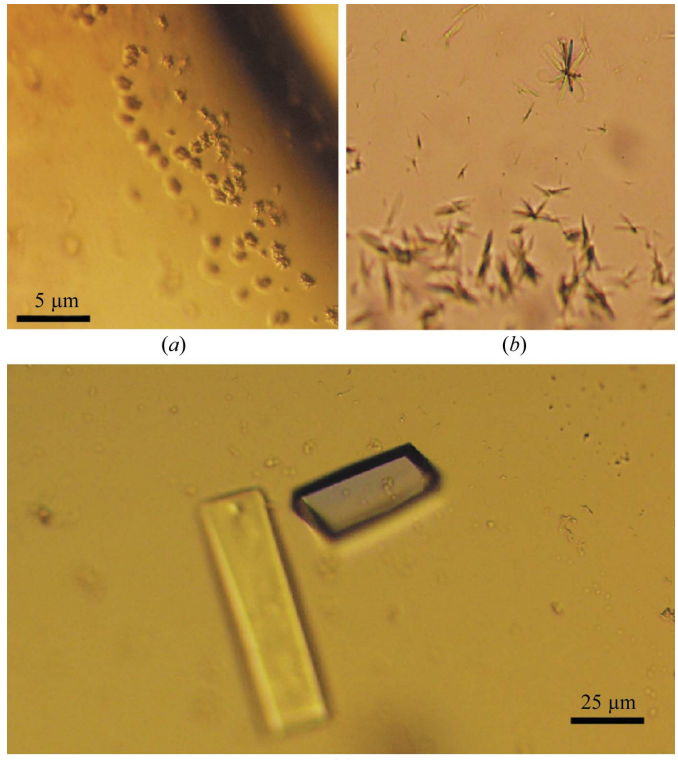

Figure 2
Crystals of the MSS4–Rab8 complex. (*a*) Crystals obtained in condition No. 36 of the PEG/Ion Screen (Hampton Research), (*b*) crystals improved by using 1,2,3-heptanetriole (Hampton Research) as an additive, (*c*) final X-ray quality crystals obtained using a combination of microseeding and macroseeding techniques.

Table 1
Crystal data and data-collection statistics for MSS4–Rab8 complex crystals.

Values in parentheses are for the highest resolution shell.

Space group	*P*1
Unit-cell parameters (Å, °)	a = 40.92, b = 49.85, c = 83.48, α = 102.88, β = 97.46, γ = 90.12
X-ray source	ESRF ID14-2
Wavelength (Å)	0.934
Resolution (Å)	19.17–2.0 (2.05–2.00)
R_{sym}	4.9 (29.1)
Total observations	85632
Unique observations	40780
Completeness (%)	94.5 (74.5)
$\langle I/\sigma(I)\rangle$	11.6 (2.9)

(Hampton Research) as an additive (Fig. 2*b*) in combination with microseeding and macroseeding techniques. Initial bundles of tiny needles were used for streak-seeding into freshly mixed drops. This was repeated iteratively until monocrystals were observed. The obtained monocrystals were then transferred to new crystallization drops, where they reached their final size. X-ray quality crystals (Fig. 2*c*) were grown in 2 µl hanging drops equilibrated against 20%(*w*/*v*) PEG 3350, 50 m*M* Tris–HCl pH 9.0, 0.2 *M* magnesium acetate, 0.15%(*w*/*v*) 1,2,3-heptanetriole. The concentration of PEG 3350 was increased to 35%(*w*/*v*) by addition of PEG 3350 to the reservoir solution after the crystals had reached their maximal size, typically 60 × 20 × 3 µm, after which the drop was allowed to equilibrate for an additional day to achieve final equilibration to allow the crystals to be fished out and frozen in liquid nitrogen without additional treatment with cryoprotectant.

2.4. Data collection and processing

Beamline ID14-2 at the ESRF (Grenoble) equipped with an ADSC Q4 CCD detector and Oxford Cryostream was used to collect 190° of data with an oscillation range of 0.7° and an exposure of 2 s with three passes per image at a crystal-to-detector distance of 190 mm and an X-ray wavelength of 0.934 Å. A protein-complex crystal of dimensions 50 × 15 × 5 µm was kept at 100 K for collection of the data set. Data to 2.0 Å resolution were processed using the *XDS* program suite (Kabsch, 1993).

3. Results and discussion

We aimed to structurally characterize the MSS4/DSS4 interaction with Rab proteins by solving the X-ray structure of one of the GEF proteins in complex with Rab. Our initial attempts to crystallize GEF–Rab complexes assembled with individually purified Rab proteins and MSS4 or DSS4 failed, mostly owing to instability of the complex. We therefore decided to use coexpression of the binding partners in order to generate the complex. For this purpose, we cloned Rab8, Ypt1 and Sec4 into the pET30a vector and MSS4 and DSS4 into the pET19 vector containing an N-terminal six-His tag followed by a tobacco etch virus protease-cleavage site. A combination of recombinant pET19 and pET30 was used to cotransform *E. coli* BL21(DE3)RIL (Novagen). Coexpression of the GEF and the Rab protein was analyzed by SDS–PAGE and complex formation was proved by a pull-down assay on a nickel–NTA HiTrap Chelating HP column (GE). We purified three complexes (DSS4–Sec4, DSS4–Ypt1 and MSS4–Rab8). The most soluble and stable complex was formed between Rab8 and MSS4. The MSS4–Rab8 complex was purified in preparative amounts using nickel-chelating and subsequent size-exclusion chromatography. Diffraction-quality crystals of the MSS4–Rab8 protein binary complex were grown by the hanging-drop method from a crystallization condition consisting of 20%(*w*/*v*) PEG 3350, 50 m*M* Tris–HCl pH 9.0, 0.2 *M* magnesium acetate, 0.15%(*w*/*v*) 1,2,3-heptanetriole using a seeding technique. To prove directly that the crystallized species is the MSS4–Rab8 complex, we washed approximately ten crystals of 60 × 20 × 3 µm in size in the reservoir solution, dissolved them and loaded the solution onto SDS–PAGE (Fig. 3). The analysis clearly showed that the crystals indeed contain both MSS4 and Rab8 proteins. The crystals belonged to space group *P*1, with unit-cell parameters a = 40.92, b = 49.85, c = 83.48 Å, α = 102.88, β = 97.46, γ = 90.12°. Statistics of data collection and processing to 2.0 Å resolution are summarized in Table 1. The Matthews coefficient V_M (Matthews, 1968) was calculated to be 2.51 Å^3 Da^{-1} for a protein-complex molecular weight of 33 kDa, suggesting the presence of two complexes in the asymmetric unit. This V_M value corresponds to a solvent content of approximately 51.1%. Structure solution of the MSS4–Rab8 complex *via* molecular replacement is currently being undertaken using the MSS4 (PDB code 1hxr) and Rab3a (PDB code 3rab) (homologous to Rab8) structures as search models.

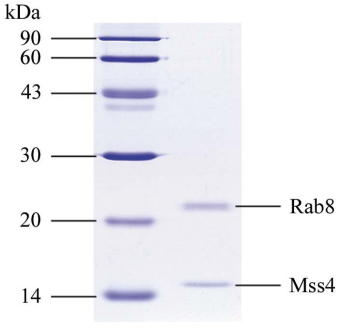

Figure 3
15% SDS–PAGE analysis of the MSS4–Rab8 complex crystals.

G. Holtermann is acknowledged for invaluable technical assistance. We thank the staff of beamline 14-2, ESRF and I. Schlichting and W. Blankenfeldt for help with data collection. Professor Dr A. Barnekow (Münster University, Germany) and Dr M. Fukuda (RIKEN, Japan) are acknowledged for generous gifts of the MSS4 and Rab8 genes, respectively. This work, as part of an award under the European Young Investigator Awards scheme (EURYI) to AR, was supported by funds from the DFG (grant RA 1364/1-1) and the EC Sixth Framework Programme coordinated by the European Science Foundation.

References

Burton, J., Burns, M. E., Gatti, E., Augustine, G. J. & De Camilli, P. (1994). *EMBO J.* **13**, 5547–5558.
Burton, J. & De Camilli, P. (1994). *Adv. Second Messenger Phosphoprotein Res.* **29**, 109–119.
Burton, J., Roberts, D., Montaldi, M., Novick, P. & De Camilli, P. (1993). *Nature (London)*, **361**, 464–467.
Colicelli, J. (2004). *Sci. STKE*, **2004**, RE13.
Collins, R. N., Brennwald, P., Garrett, M., Lauring, A. & Novick, P. (1997). *J. Biol. Chem.* **272**, 18281–18289.
Eathiraj, S., Pan, X., Ritacco, C. & Lambright, D. G. (2005). *Nature (London)*, **436**, 415–419.
Kabsch, W. (1993). *J. Appl. Cryst.* **26**, 795–800.
Lazar, T., Gotte, M. & Gallwitz, D. (1997). *Trends Biochem. Sci.* **22**, 468–472.
Matthews, B. W. (1968). *J. Mol. Biol.* **33**, 491–497.
Novick, P. & Zerial, M. (1997). *Curr. Opin. Cell Biol.* **9**, 496–504.
Rak, A., Fedorov, R., Alexandrov, K., Albert, S., Goody, R. S., Gallwitz, D. & Scheidig, A. J. (2000). *EMBO J.* **19**, 5105–5113.

Rak, A., Pylypenko, O., Durek, T., Watzke, A., Kushnir, S., Brunsveld, L., Waldmann, H., Goody, R. S. & Alexandrov, K. (2003). *Science*, **302**, 646–650.
Rak, A., Pylypenko, O., Niculae, A., Pyatkov, K., Goody, R. S. & Alexandrov, K. (2004). *Cell*, **117**, 749–760.
Stein, M. P., Dong, J. & Wandinger-Ness, A. (2003). *Adv. Drug Deliv. Rev.* **55**, 1421–1437.
Waters, M. G. & Pfeffer, S. R. (1999). *Curr. Opin. Cell Biol.* **11**, 453–459.
Yu, H. & Schreiber, S. L. (1995*a*). *Biochemistry*, **34**, 9103–9110.
Yu, H. & Schreiber, S. L. (1995*b*). *Nature (London)*, **376**, 788–791.
Zhu, Z., Delprato, A., Merithew, E. & Lambright, D. G. (2001*a*). *Biochemistry*, **40**, 15699–15706.
Zhu, Z., Dumas, J. J., Lietzke, S. E. & Lambright, D. G. (2001*b*). *Biochemistry*, **40**, 3027–3036.